Turkish Journal of Electrical Engineering & Computer Sciences

http://journals.tubitak.gov.tr/elektrik/

Research Article

Turk J Elec Eng & Comp Sci
(2017) 25: 1657 – 1668

doi:10.3906/elk-1603-198

Design of a self-starting hybrid permanent magnet hysteresis synchronous motor connected directly to the grid

Mehmet GEDİKPINAR*, Ömür AYDOĞMUŞ
Department of Electrical and Electronics Engineering, Faculty of Technology, Fırat University, Elazığ, Turkey

Received: 17.03.2016 • **Accepted/Published Online:** 08.06.2016 • **Final Version:** 29.05.2017

Abstract: In this work, a permanent magnet hysteresis synchronous (PMHS) motor was designed to improve the efficiency of the system. The proposed motor is intended for pumping applications, such as submersible pump motors, fire pumps, oil-well pumps, and circulation pumps requiring high-speed operation. The efficiency of the pump system increases depending on the speed of the pump fans. The total efficiency of the pump system is reduced because the load increases exponentially in these types of application systems. The speed is important for the pumping applications in order to improve the efficiency of the pump system. Nowadays, traditional induction motors are widely used in these applications; however, they experience rotor slip when operating under synchronous speed with loaded conditions. The system efficiency is dramatically reduced when the rotor slip is increased by depending on the pump load. The proposed motor can achieve self-starting without any kind of driver for direct connection to the grid. In addition, the proposed motor can be operated at synchronous speed under full load conditions. The designed motor is analyzed by using simulation results, such as the performance of the starting motor at various loads, stator-rotor flux density, and synchronous speed at stand-still.

Key words: Hybrid rotor, hysteresis, motors, permanent magnet, self-starting

1. Introduction

Producing/using more efficient systems has become mandatory due to increased consumption of electricity and limited energy resources. Electric motors consume the most electrical power in industrial applications, as well as home appliances and hand tools. In particular, single-phase induction motors are widely used in low-power industrial machines, home applications, and many applications on a single-phase network. These motors have very low efficiency, take up more space, and consume more electrical power than other electric motors. However, the single-phase induction motor requires auxiliary equipment to operate. Nowadays, a type of synchronous motor is used with a magnet rotor to improve the efficiency of the system. In particular, the permanent magnet synchronous motor (PMSM) and brushless DC motor (BLDC) are used for obtaining higher efficiency, power/weight ratio, torque/inertia ratio, and smoother torque at low speeds. However, these types of motors require drive systems, which have high cost and high space volume requirements. The two-level voltage source inverters are widely used for controlling the PMSM and BLDC. However, the inverters have several disadvantages, such as requiring large DC-link capacitors and rectifiers, lacking bidirectional power flow, requiring a large input filter for obtaining low total harmonic distortion (THD), and having no four-quadrant operating ability. The hysteresis motors can be used to circumvent these disadvantages. They have reliable

*Correspondence: mgedikpinar@firat.edu.tr

self-starting without need for any kind of start-up procedure; a durable windingless rotor structure; high output power/unit volume; smooth, vibration-free operation; quiet operation; nonzero torque at rest; constant torque; and low inrush current [1–5]. There are also various studies to be found in the literature [6–8] on line-start permanent magnet synchronous motors without using the hysteresis ring.

The measurement of the rotor position is not necessary for starting and synchronization, unlike other synchronous motors [9,10]. On the other hand, the rotor losses are very low in comparison to induction motors. Since there is no slip speed when running, there are no slip losses of the rotor. However, the performance of a PMHS motor suffers from rotor harmonic losses. PMHS motors need a large magnetizing current due to the requirement of the magneto-motor force. Permanent magnets can be added to the rotor system of a traditional hysteresis motor to increase torque. The mutual torque is developed between the stator winding and the magnets, with induction torque occurring in the hysteresis ring. All the torques, such as hysteresis, mutual, and induction torque, are active in the initial case. The induction torque does not appear in the steady-state case on account of the synchronous speed. In that case, the induction torque cannot be developed by the free-rotor slip operation [11,12].

Traditional induction motors are commonly used for submersible pump motors, fire pumps, jet pumps, oil well pumps, and circulation pumps. The speed of the pump fans is dramatically reduced due to induction motors having rotor slip at load conditions. Hence, the total efficiency of the pump system is reduced because the load increases exponentially. The rotor slip increases depending on the pump load. The speed is more important for pumping applications to improve the efficiency of the pump system. To increase the system's efficiency, the synchronous speed operation of the motor gains importance in these applications. Therefore, in this study, a synchronous motor is used to address the rotor slip problems.

The structure of the stator and rotor of the proposed PMHS motor is given in Figure 1. The stator uses a traditional three-phase AC stator lamination structure, although the rotor structure does not look like a traditional hysteresis rotor. The proposed rotor has two hysteresis rings: the inner hysteresis ring and the outer hysteresis ring. The magnets are located between the two hysteresis rings, as shown in Figure 1. This rotor type can be called a 'sandwich rotor'.

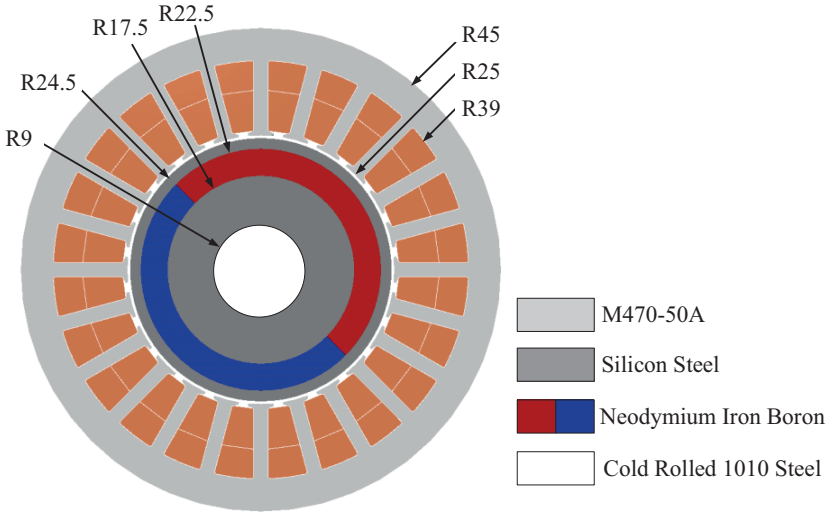

Figure 1. Layout of stator and rotor structure.

This paper presents a novel rotor structure for self-starting, connected directly to the grid without use of

any kind of drive system. Additionally, the proposed motor does not require a starting procedure or knowledge of the rotor position. Thus, the total cost of the system and its volume can be considerably reduced by using the purposed motor. The proposed PMHS motor was designed and analyzed using MotorSolve/Infolytica. The designed motor was tested in order to show the performance of the grid-connected state by using the MATLAB environment. Satisfactory results were obtained for various load conditions, which are presented in this paper.

2. Modeling of the hysteresis motor

Some assumptions are considered when regarding the hysteresis motor model, such as balanced sinusoidal distributed winding, and the assumption that the permeability of the hysteresis material is constant. A constant current source I_m is used for modeling the permanent magnet. Resistance R is used to represent the effect of the eddy current. Hysteresis resistance R_h and an equivalent hysteresis inductance L_h are used to show the hysteresis effect. R_h and L_h are functions of the hysteresis lag angle δ. The hysteresis ring has two parts, an inner and an outer, so the resistances and inductances can be represented by Eqs. (1)–(4). The calculation of magnetizing inductance is given in Eq. (5). The equivalent circuits of the resistance and inductance are relevant for use in the dq-model. The equivalent circuits of the resistances are determined as Re_{eq} and Rh_{eq}. The equivalent circuits of the inductances are determined as Le_{eq} and Lh_{eq}.

$$R_{h_{(inner)}} = \frac{3K_w^2 N_w^2 V_{h_{(inner)}} \mu}{\mu^2 r_{r_{(inner)}}} sin\delta \tag{1}$$

$$R_{h_{(outer)}} = \frac{3K_w^2 N_w^2 V_{h_{(outer)}} \mu}{\mu^2 r_{r_{(outer)}}} sin\delta \tag{2}$$

$$L_{h_{(inner)}} = \frac{3K_w^2 N_w^2 V_{h_{(inner)}} \mu}{\mu^2 r_{r_{(inner)}}} cos\delta \tag{3}$$

$$L_{h_{(outer)}} = \frac{3K_w^2 N_w^2 V_{h_{(outer)}} \mu}{\mu^2 r_{r_{(outer)}}} cos\delta \tag{4}$$

$$L_m = \frac{6K_w^2 N_w^2 V_{h_{(inner)}} \mu_0 r_g l}{\pi p^2 l_g} \tag{5}$$

Here, ω_b is base angular frequency, V_h is the volume of the hysteresis ring, r_r is the average radius of the hysteresis ring, r_g is the mean radius of the air gap, and l_g is the radial length of the air gap. L_{mq} and L_{md} are assumed equal to L_m due to the nonsalient rotor.

There are two components in the model, which are hysteresis and eddy current resistances, as shown in Figure 2. The first resistance expresses the hysteresis loss sR_h, and the second represents the eddy current loss R_e, which occurs in the rotor. The other resistance represents the output power of the motor. s is the slip of the motor, $((1--s)/s)R_e$ is the effective eddy current, and $(1--s)R_h$ is the hysteresis resistances. These rotor losses only occur under the synchronous speed. High I^2R losses occur in the rotor when the motor is in starting operation, so the rotor speed should reach synchronous speed as soon as possible. The motor torque is thoroughly developed with both a permanent magnet and hysteresis effects at synchronous speed [13].

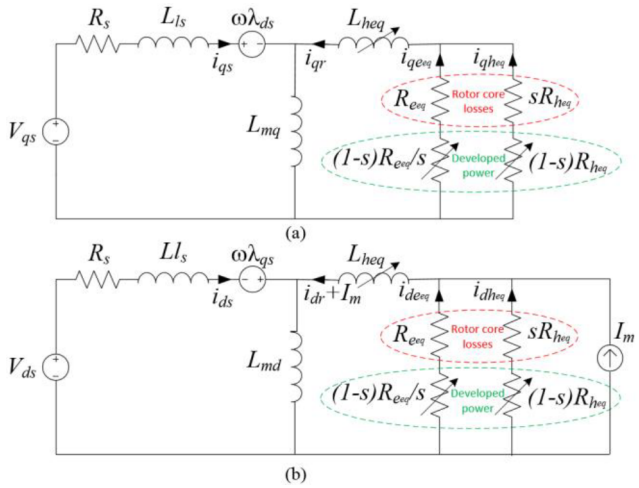

Figure 2. Electrical equivalent circuits: (a) q-axis, (b) d-axis.

The dq-axis equations of the motor are derived from the equivalent circuits and are expressed as in [14]. The dq-model voltages of the stator and rotor result from Eqs. (6)–(9). Otherwise, the flux linkages of the motor can be determined by using Eqs. (10)–(13).

$$V_{qs} = R_s I_{qs} + \frac{d\lambda_{qs}}{dt} + \omega_r \lambda_{ds} \tag{6}$$

$$V_{ds} = R_s I_{ds} + \frac{d\lambda_{ds}}{dt} - \omega_r \lambda_{qs} \tag{7}$$

$$V_{qr} = R_r I_{qr} + \frac{d\lambda_{qr}}{dt} = 0 \tag{8}$$

$$V_{dr} = R_r I_{dr} + \frac{d\lambda_{dr}}{dt} = 0 \tag{9}$$

$$\lambda_{qs} = I_{qs}\left(L_{mq} + L_{ls}\right) + L_{mq}\left(I_{qe_{eq}} + I_{qh_{eq}}\right) \tag{10}$$

$$\lambda_{ds} = I_{ds}\left(L_{md} + L_{ls}\right) + L_{md}\left(I_{de_{eq}} + I_{dh_{eq}} + I_m\right) \tag{11}$$

$$\lambda_{qr} = \left(I_{qe_{eq}} + I_{qh_{eq}}\right)\left(L_{h_{eq}} + L_{mq}\right) + L_{mq} I_{qs} \tag{12}$$

$$\lambda_{dr} = \left(I_{de_{eq}} + I_{dh_{eq}}\right)\left(L_{h_{eq}} + L_{md}\right) + L_{md}\left(I_{ds} + I_m\right) \tag{13}$$

$$T_e = \frac{3}{2} p\left(\lambda_{ds} I_{qs} - \lambda_{qs} I_{ds}\right) \tag{14}$$

Here, R_s is the stator phase resistance, L_{ls} is the per-phase stator leakage inductance, L_{mq} and L_{md} are respectively the q-d axis magnetizing inductances, and ω_r is the electrical angular speed of the rotor. V_{qs} and V_{ds} are the q-d axis stator voltages, V_{qr} and V_{dr} are the q-d axis rotor induced voltages, λ_{qs} and λ_{ds} are the q-d axis stator flux linkages, λ_{qr} and λ_{dr} are the q-d axis rotor flux linkages, and T_e is the developed torque.

3. Design of the PMHS motor

The proposed motor is designed using MotorSolve. The stator is taken as a standard structure, as shown in Figure 3. The proposed motor is shown in Figure 3 with lamination of the stator, which has a traditional form; windings of the stator, which has standard copper wire; air gap (Δda = 0.5 mm); outer ring rotor (Δdo = 2 mm), which is important for operating in hysteresis mode; inner ring of the rotor (Δdi = 9 mm); shaft (1010 stainless steel magnetic material); and magnet of the rotor (L = 140 mm). The stator lamination material is taken as M470-50A, and the stator skew angle is given as approximately 0° to obtain a simple structure. The winding layout is given in Table 1. The stator slots are given as 24, and the stator winding is taken as double layer. The number of coils per set is selected as 1, and the coil span is taken as 12. The number of coil turns is taken as 24. The slot fill factor is calculated as approximately 54%. The stack length of the stator is taken as 140 mm, which is a compact design. Furthermore, the proposed motor has approximately three times higher power/volume than a traditional induction motor with the same outer diameter of the stator and stack length.

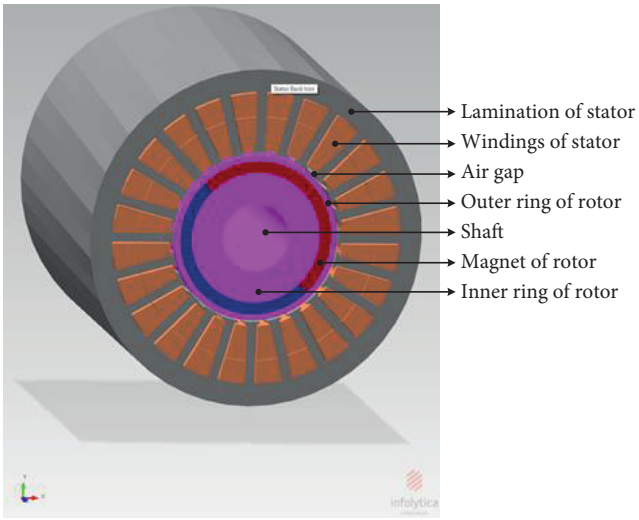

Figure 3. The structure of the rotor and stator.

Table 1. Stator winding layout for phase A.

	Coil	Go	Return
Layout of phase A	1	1	13
	2	2	14
	3	3	15
	4	24	12
	5	1	13
	6	2	14
	7	3	15
	8	24	12

The structure of the stator and rotor of the proposed motor is illustrated in Figure 3. The rotor has two hysteresis rings: an inner hysteresis ring and an outer hysteresis ring. The material of the rings has been determined as silicon (electrical) steel because of its advantages, including reduced iron losses, increased magnetic induction, and ability for higher frequency operation. The shaft material is taken as 1010 stainless

steel, which is a magnetic material. The magnet is located between two hysteresis rings, as shown in Figure 3. The magnet material selected is neodymium iron boron (28/32). The rotor type can be referred to as a sandwich rotor. The width of the outer ring should be thin for high torque and quick-starting.

The magnetic flux density is axial in the air gap and inner and outer rotor hysteresis rings, but it is radial in the permanent magnet. The maximum flux density occurred on the magnetic stator pole axis and the junction of the rotor magnet poles, as shown in Figure 4. The outer hysteresis ring and the air gap have the same flux orientation (Figure 4). In particular, the thickness of the outer ring of the rotor plays an important role in the flux orientation of hysteresis. The optimum thickness of the ring has been selected by trying different sizes, and it was determined to be 2 mm. The self-starting/synchronization of the proposed motor can only be obtained by optimum thickness. The maximum value of the flux density is 2.68 T at the joint of the two magnet pole surfaces. The two magnets are adjoined in order to eliminate the eddy flux that reduces the generated torque of the rotor. The inner ring is used to provide the flux loop. The form of flux orientation is smoothly generated, and there is no flux leakage in the stator and rotor. The hysteresis effects are shown especially in the rings. In addition, there is no flux leakage in the shaft, since the shaft material was selected as a nonmagnetic material (1010 stainless steel). At the same time, the shaft has no buffer role as the hub of the rotor. The diameter of the shaft plays an important role for mechanical durability. In this case, the shaft of the rotor cannot be reduced because of the high power/volume.

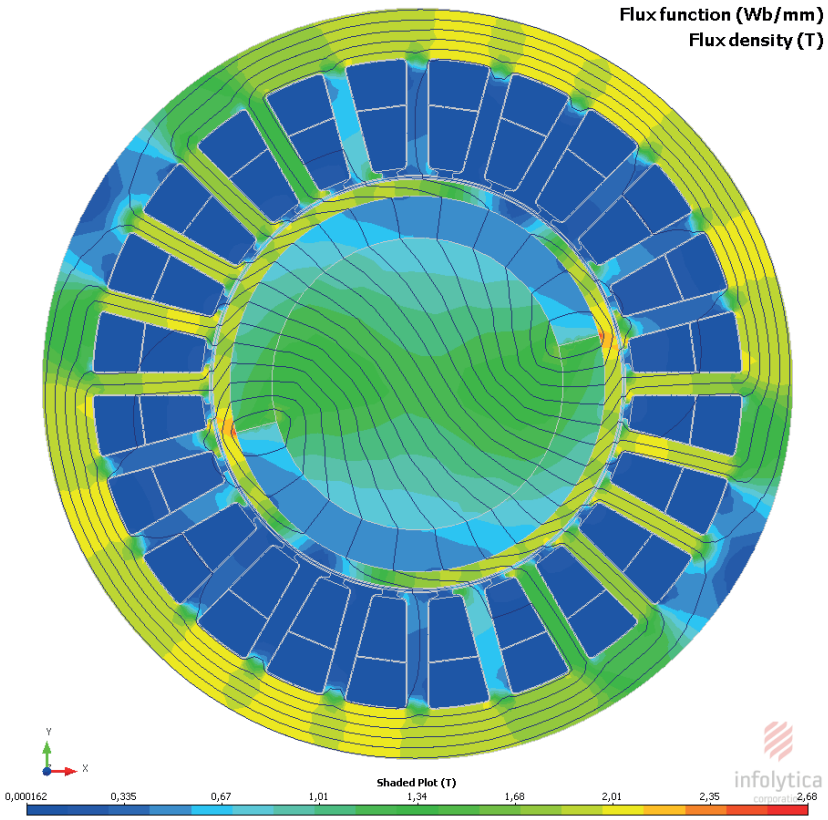

Figure 4. The flux density of the motor.

4. Performance results of the PMHS motor

The proposed motor was tested for no-load, full load, and overload by using the MATLAB/Simulink blocks, as seen in Figure 5. Because starting connected directly to the grid cannot be achieved by using the motor design program, MATLAB was utilized. The motor was connected directly to the grid for self-starting conditions under various loads, and especially pump load.

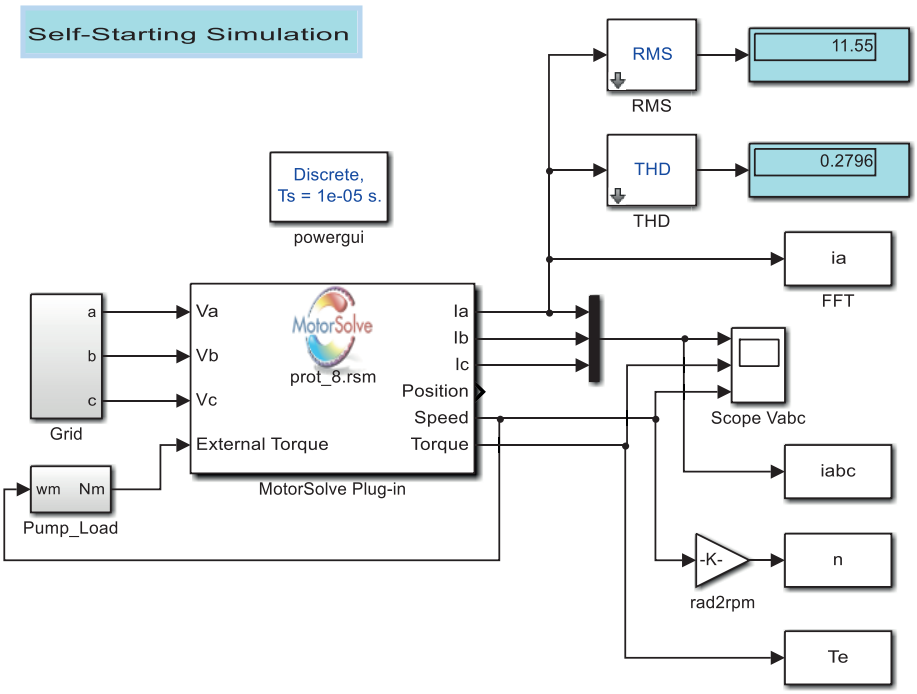

Figure 5. Block diagram of the motor test system for MATLAB/Simulink.

It can be noted that the break-down point of the torque occurred over synchronous speed. The design program cannot support the connection to the grid for motor testing. The design program only supports the hysteresis current controller and vector controller to obtain the torque-speed curve. The rapid and accurate results are based on automated finite element analysis (FEA) simulations. However, the proposed motor does not require any kind of controller in the real operation. Therefore, a MATLAB-based motor model was used, which was developed by a commercial design program (MotorSolve/Infolytica) in order to obtain the grid connection structure. In addition, use of the MATLAB motor model allows for transient and steady-state analyses. The results are obtained by using both MATLAB and MotorSolve, as illustrated in the figure descriptions.

The first operation is taken for pump load conditions, as shown in Figure 6. The pump load is modeled as assumed quadratic, which depends on the mechanical speed of the motor. The characteristics of the pump load include both inherently no-load and full load conditions. The stator currents, motor speed, and torque are shown in Figures 6a, 6b, and 6c, respectively.

It can be noted that the synchronization was provided in a short amount of time, approximately 100 ms, as shown in Figure 6b. The obtained speed of the motor has low ripples at synchronous speed. In addition, the torque ripples are low under the same conditions, as shown in Figure 6c. Furthermore, the value of the nominal torque is determined as 17.5 Nm. The rated torque corresponds to approximately 5.5 kW of output power of the motor. The stator currents have some distortions due to the saturation of the stator lamination material.

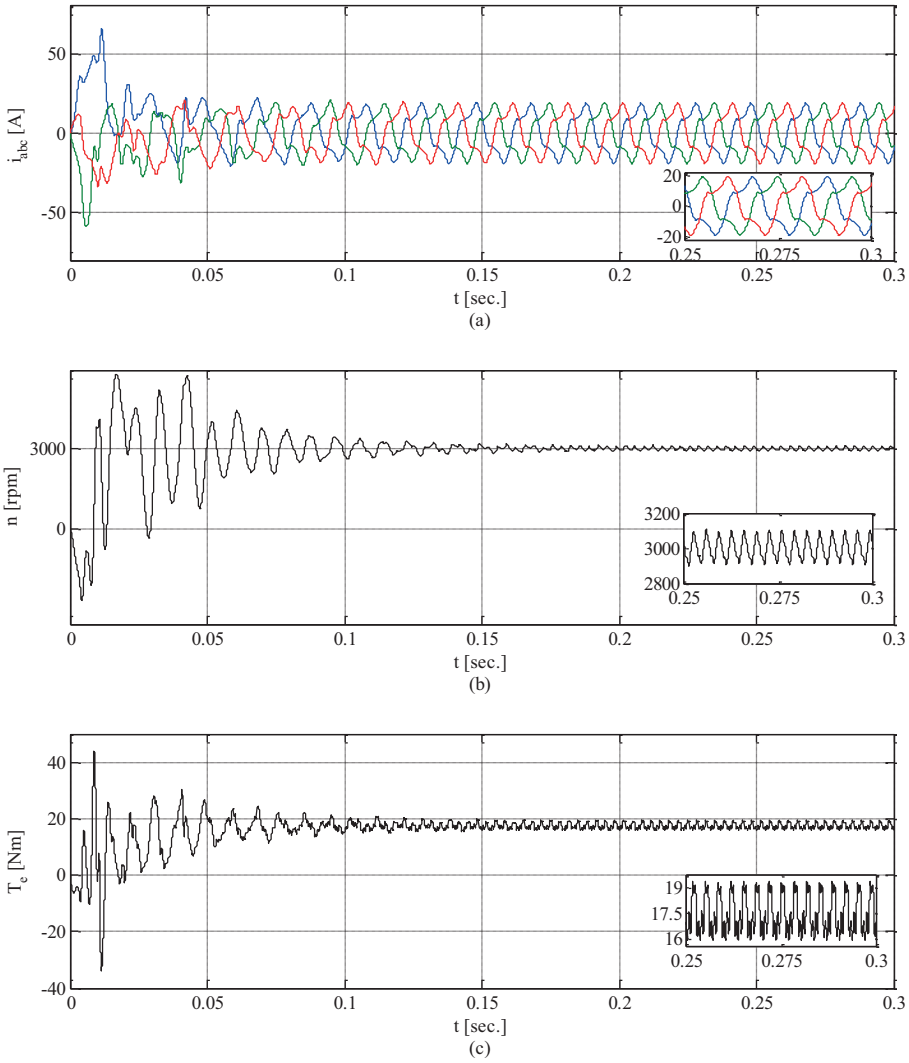

Figure 6. Pump load (T_{max} = 17.5 Nm) conditions: a) stator currents, b) motor speed, c) shaft torque.

The curve of the stator current/THD torque is illustrated in Figure 7. The critical torque value was determined at about 30 Nm. The nominal torque of the motor can be seen in the figure and is illustrated as maximum (17.5 Nm) over the torque axis. The details of the curves are shown in Table 2. The curves show that the results of the various load conditions are satisfactory for the motor design.

Table 2. Rated values.

Torque (Nm)	I_{rms} (A)	I_{rms} THD (%)
8.75	9.62	4.35 (half)
10	9.66	6.55
15	10.64	21.70
17.5	11.55	27.96 (max.)
20	12.71	32.94
25	15.68	40.02
30.625	20.4	41.00 (break down)

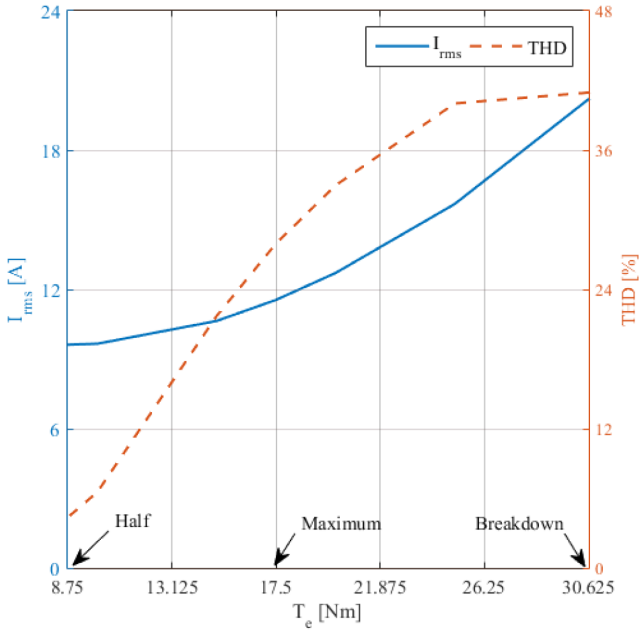

Figure 7. Curves of the rated values (current, torque, and THD of the stator current).

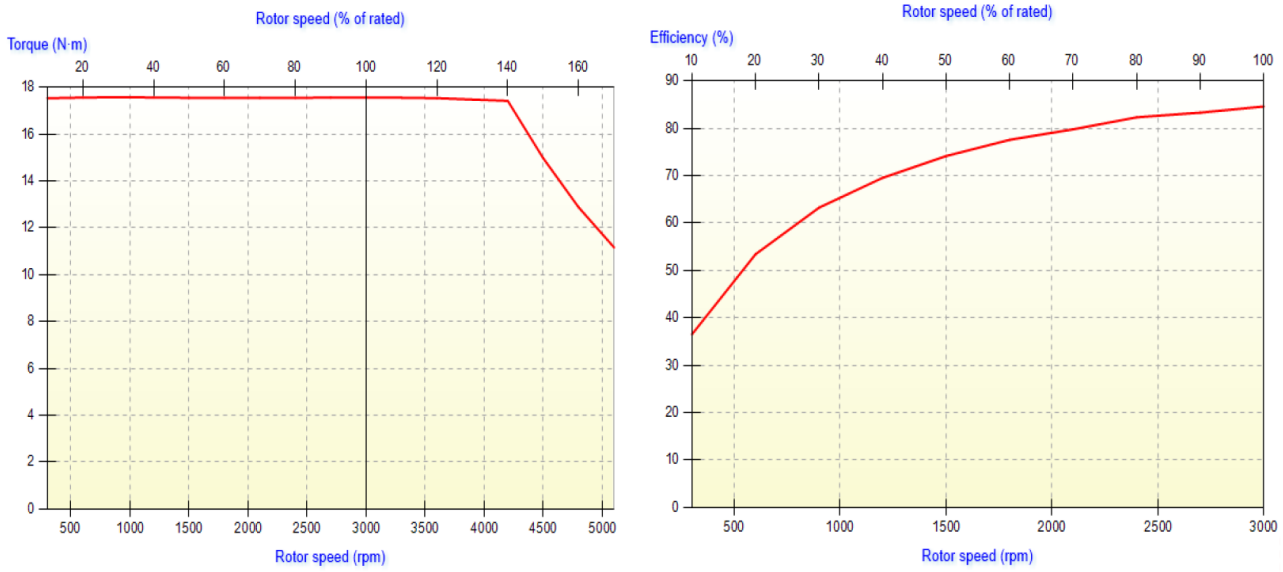

Figure 8. Left: speed-torque curve; right: speed efficiency.

The curve of the speed-torque is given in Figure 8 (left). The rated speed of the motor was determined as 3000 rpm. Nevertheless, the motor can operate at up to 4250 rpm (140%, in Figure 8 (left)), and the motor can develop torque of 17.5 Nm at the nominal speed as shown in Figure 8 (right). Despite low motor efficiency at low speed, it is about 85.3% at the nominal speed. The outer ring operates as eddy current condition up to nominal speed, due to low efficiency when under 3000 rpm. This case is not important for the proposed motor, because the motor operates at the synchronous speed, and this eddy current disappears at the synchronous speed. Thus, motor efficiency is increased at this speed.

The stator current that relates to the U phase was analyzed with the harmonic spectrum for half-load and full load, as shown in Figure 10. The THD of the current waveform is low at the level of a low load. For instance, the current THD is calculated as 4.37% for half-load condition. This is an appropriate value for the motor applications. The current saturates when the motor load increases, because the stator lamination cannot allow more flow of the flux-line. The third harmonic is the dominant harmonic order.

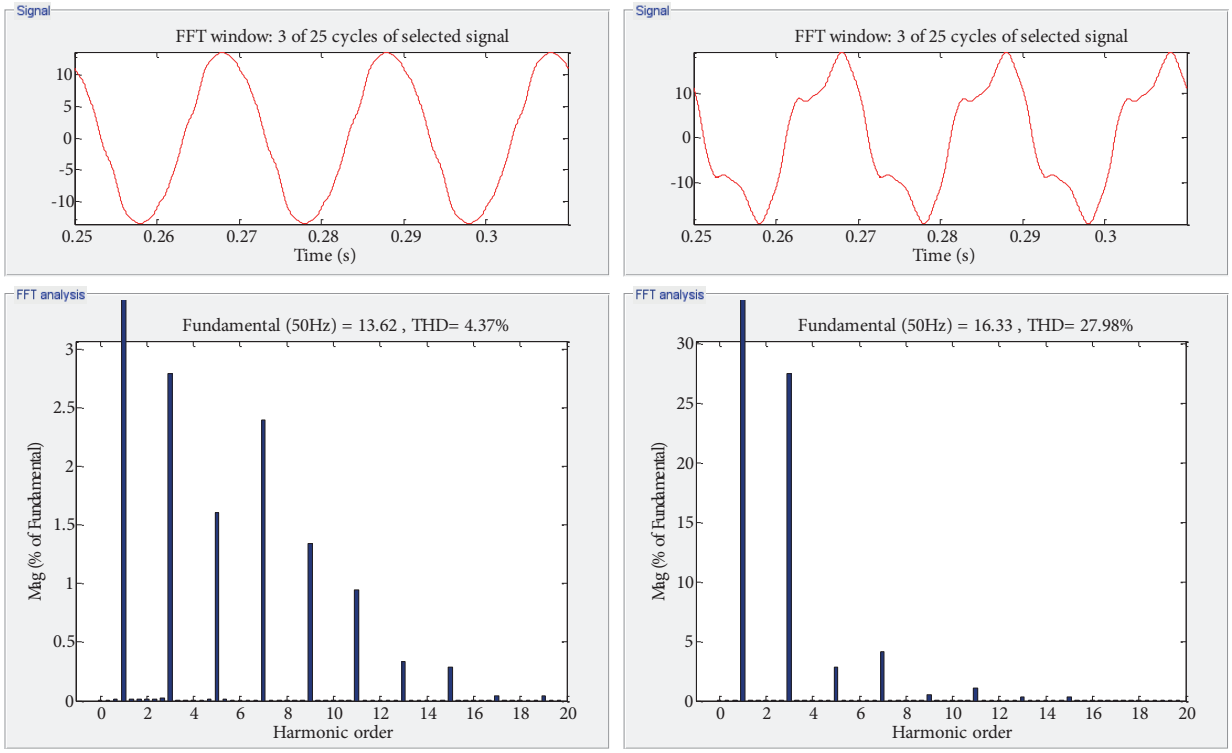

Figure 9. Current and its harmonic spectrum. Left: half-load; right: full load.

The motor does not have the ability to start directly under nominal torque conditions. However, it can be directly started at 15.2 Nm, which is 86% of the nominal torque. The synchronization capability of the motor has been tested with a step load from 15.2 Nm to 0 Nm, as shown in Figure 10.

5. Conclusions

A novel rotor design was presented for the three-phase hybrid PMHS motor with inset cylindrical magnet. The shapes of both the magnet and rotor core are different from those seen in the published literature. A cylindrical hole magnet is used for structural durability and to avoid the eddy flux between the end of poles N and S. The proposed motor can achieve self-starting without any kind of driver for directly connecting to the grid. Furthermore, the purposed motor does not require a starting procedure or knowledge of the rotor position. Moreover, the purposed motor can operate at synchronous speed due to the synchronous rotor structure not having any kind of drive system. The designed motor was analyzed to show the performance when starting with various constant loads and pump load. Satisfactory performances were obtained under various load conditions. One of the most important properties observed was that the rotor speed quickly reached synchronous speed (about 100 ms).

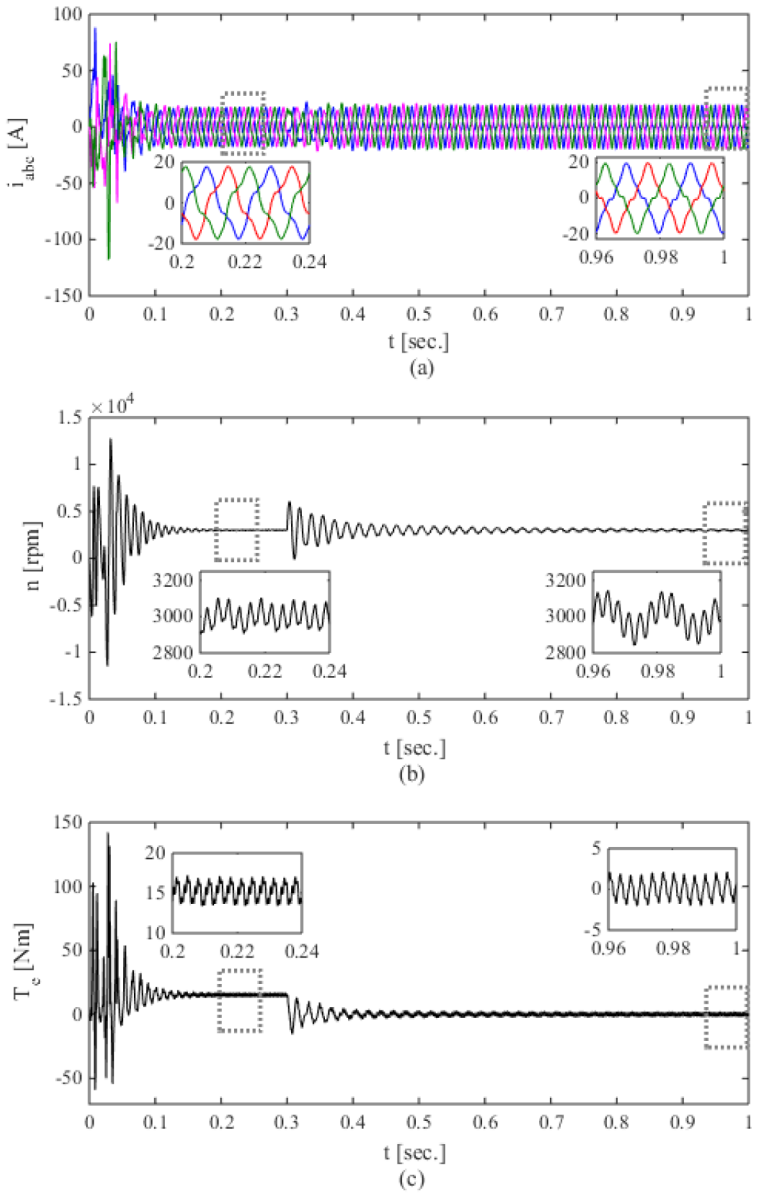

Figure 10. Synchronization capability of the motor at the step load condition from 15.2Nm to 0Nm a) Stator currents, b) Motor speed, c) Shaft Torque.

The efficiency of the pump systems increases with the speed of the pump fans. Compared to a traditional pump fed by induction motor, the operating speed can be increased from 2800 to 3000 rpm by using the proposed motor. The shaft power of the motor can be calculated by multiplication of the angular speed and torque. The additional power increases the total efficiency of the pump. The proposed motor is especially appropriate for pumping applications such as submersible pump motors, fire pumps, jet pumps, oil-well pumps, and circulation pumps requiring high speed. In subsequent research studies, the number of slots and their shapes will be improved in order to eliminate stator harmonics and reduce torque ripples. The proposed motor has been compared with an induction motor, which is given in Table 3.

Table 3. Comparison between the induction motor and proposed motor.

	4″ Submersible pump motor	
Rated values	Induction motor (Franklin Electric)	Proposed motor
Power (W)	5500	5500
Voltage (V)	380	380
Current (A)	13	11.55
Power factor	0.85	0.84
Efficiency (%)	75	85
Frequency (Hz)	50	50
Shaft speed (rpm)	2875	3000
Torque ripple	$\approx 3\%$	$\approx 10\%$
Current THD	$\approx 4\%$	$\approx 27\%$

References

[1] Cardwell DA, Ginle DS. Handbook of Superconducting Materials. Boca Raton, FL, USA: CRC Press, 2002.

[2] Nitao JJ, Scharlemann, ET, Kirkendall BA. Equivalent Circuit Modeling of Hysteresis Motors. Livermore, CA, USA: Lawrence Livermore National Laboratory, 2009.

[3] Jagiela M, Garbiec T, Kowol. Design of high-speed hybrid hysteresis motor rotor using finite element model and decision process. IEEE T Magnet 2014; 50: 861-864.

[4] Qin R, Rahman MA. Magnetic Equivalent circuit of PM hysteresis synchronous motor. IEEE T Magnet 2003; 39: 2998-3000.

[5] Darabi A, Mohsen SM, Ghanbari T. Coreless dual-rotor disc hysteresis motor, modeling, and performance prediction. Elect Power Compon Syst 2010; 38: 575-591.

[6] Ugale RT, Chaudhari BN, Baka S, Pramanik A. A hybrid interior rotor high-performance line start permanent magnet synchronous motor. Elect Power Compon Syst 2014; 42: 901-913.

[7] Azari MN, Mirsalim M. Performance analysis of a line start permanent magnet motor with slots on solid rotor using finite element method. Elect Power Compon Syst 2013; 41: 1159-1172.

[8] Boroujeni ST, Haghparast M, Bianchi N. Optimization of flux barriers of line-start synchronous reluctance motors for transient- and steady-state operation. Elect Power Compon Syst 2015; 43: 594-606.

[9] Rahman MA, Qin R. A permanent magnet hysteresis hybrid synchronous motor for electric vehicles. IEEE T Ind Electron 1997; 44: 46-53.

[10] Qian J, Rahman MA. Analysis of field oriented control for permanent magnet hysteresis synchronous motors. IEEE T Ind Appl 1993; 29: 1156-1163.

[11] Rahman MA, Copeland MA, Slemon GR. An analysis of the hysteresis motor part III: parasitic losses. IEEE T Power Appl 1969; 88: 954-961.

[12] Kurihara K, Rahman MA. Transient performance analysis for permanent-magnet hysteresis synchronous motor. IEEE T Ind Appl 2004; 40: 135-142.

[13] Rabbi SF, Rahman MA. Equivalent circuit modeling of an interior permanent magnet hysteresis motor. IEEE 2014 Conference on Electrical and Computer Engineering; 4–7 May 2014; Toronto, Canada. New York, NY, USA: IEEE. pp. 1-5.

[14] Rahman MA, Qin R. Starting and synchronization of permanent magnet hysteresis motors. IEEE T Ind Appl 1996; 32: 1183-1189.